Click Here for Full Article

Simulation of the eastward 4-day wave in the Antarctic winter mesosphere using a gravity wave resolving general circulation model

Shingo Watanabe,[1] Yoshihiro Tomikawa,[2] Kaoru Sato,[3] Yoshio Kawatani,[1] Kazuyuki Miyazaki,[1] and Masaaki Takahashi[4]

[1] The eastward moving 4-day wave in the Antarctic winter mesosphere is investigated using a high-resolution middle atmosphere general circulation model that directly simulates the spontaneous generation, propagation, and dissipation of gravity waves. The results are also compared with the simulated seasonal march of the meridional structures of the westerly jet streams in the Southern Hemisphere upper stratosphere and mesosphere in order to investigate baroclinic/barotropic instability as a possible excitation mechanism for the 4-day wave. The model successfully reproduces the dynamically unstable double-jet structure of the mesospheric westerly winds. The simulated 4-day wave develops in association with the baroclinic and barotropic instability of the mesospheric mean flows and has similar characteristics to those observed at $50-60°$S near the stratopause. The 4-day wave has strong equatorward heat flux associated with strong baroclinicity in the Antarctic winter mesosphere, mainly attributable to poleward overturning circulation driven by gravity wave forcing. Eastward forcing due to the 4-day wave occurs within the double-jet structure and offsets part of the westward forcing due to gravity waves. Such an effect partially acts to stabilize the unstable mean flow structure in the Antarctic winter mesosphere.

Citation: Watanabe, S., Y. Tomikawa, K. Sato, Y. Kawatani, K. Miyazaki, and M. Takahashi (2009), Simulation of the eastward 4-day wave in the Antarctic winter mesosphere using a gravity wave resolving general circulation model, *J. Geophys. Res.*, *114*, D16111, doi:10.1029/2008JD011636.

1. Introduction

[2] The eastward moving 4-day wave is a characteristic feature of the winter polar upper stratosphere that has been observed via satellite measurements of brightness temperatures [*Venne and Stanford*, 1979, 1982; *Prata*, 1984; *Lait and Stanford*, 1988; *Manney*, 1991; *Randel and Lait*, 1991]. The 4-day wave has also been observed in the mesosphere [*Lawrence et al.*, 1995; *Lawrence and Randel*, 1996; *Garcia et al.*, 2005; *Merzlyakov and Pancheva*, 2007] and in stratospheric tracer fields such as ozone, methane, and water vapor [e.g., *Allen et al.*, 1997; *Manney et al.*, 1998]. The 4-day wave is a planetary-scale phenomenon with zonal wave numbers (k) of $1-4$, and propagates eastward with approximately the same phase speed such that the $k = 1$ wave has a period of near 4 days, while the $k = 2$ wave has a period of near 2 days. Superposition of these wave components sometimes creates long-lived "warm pools" that circle eastward around the winter pole with a period of approximately 4 days [e.g.,

Prata, 1984; *Lait and Stanford*, 1988; *Allen et al.*, 1997]. The period of the 4-day wave is variable and shorter in the Southern Hemisphere than that in the Northern Hemisphere [*Venne and Stanford*, 1982]. In the Antarctic upper stratosphere, the period of the wave varies from approximately 3 to 5 days, probably under the influence of advection by mean winds [*Manney*, 1991]. The horizontal and vertical phase structures of the 4-day wave are also variable. The horizontal phase structure is characterized by either equatorward or poleward momentum flux. The vertical phase structure in the stratosphere generally has an equivalent barotropic structure with small vertical phase tilting, while a few events has been reported that exhibit strong equatorward heat flux [*Randel and Lait*, 1991; *Manney*, 1991].

[3] A number of studies have suggested that the 4-day wave develops in the large-scale zonal mean westerly wind with a negative potential vorticity gradient in the vicinity of the wintertime polar vortex [e.g., *Hartmann*, 1983; *Manney et al.*, 1988; *Manney*, 1991; *Randel and Lait*, 1991; *Manney and Randel*, 1993]. Two kinds of flow instabilities have been proposed to explain the observed relationships between the characteristics of the 4-day wave and the background zonal mean zonal wind; barotropic instability developing near the poleward flank of the stratospheric polar night jet, and mixed baroclinic and barotropic instability associated with the "double-jet" structure of the mesospheric westerly winds. The former case explains the equivalent barotropic structure of the 4-day wave with poleward momentum flux

[1]Frontier Research Center for Global Change, Japan Agency for Marine-Earth Science and Technology, Yokohama, Japan.
[2]National Institute of Polar Research, Tokyo, Japan.
[3]Department of Earth and Planetary Science, Graduate School of Science, University of Tokyo, Tokyo, Japan.
[4]Center for Climate System Research, University of Tokyo, Kashiwa, Japan.

confined to polar latitudes [e.g., *Hartmann*, 1983; *Manney et al.*, 1988; *Manney*, 1991], while the latter explains the significant equatorward heat flux [e.g., *Manney*, 1991; *Randel and Lait*, 1991; *Manney and Randel*, 1993].

[4] The double-jet structure has proven to be difficult to successfully reproduce in general circulation models (GCMs), primarily because momentum deposition due to small-scale upward propagating gravity waves, essential for the maintenance of large-scale flow structures in the mesosphere, has yet to be correctly resolved by GCMs [e.g., *McLandress*, 1998; *Fritts and Alexander*, 2003]. Although ongoing efforts to constrain gravity wave drag parameterizations may help to resolve these problems in the near future [e.g., *Ern et al.*, 2004, 2006; *Alexander and Barnet*, 2007; *Alexander et al.*, 2008; *Preusse et al.*, 2006, 2009], only a few low-resolution GCMs can currently reproduce the double-jet structure in the Southern Hemisphere winter mesosphere [e.g., *McLandress and Scinocca*, 2005; *Watanabe*, 2008].

[5] Recently, *Watanabe et al.* [2008] described the general features of the T213L256 middle atmosphere GCM, in which certain aspects of atmospheric gravity waves are simulated directly. In the high-resolution GCM, gravity waves are spontaneously generated by various source mechanisms, propagate laterally and vertically to reach the mesosphere, and deposit momentum during dissipation due mainly to wave breaking and critical level absorption. The momentum deposition due to the directly simulated gravity waves creates the characteristic double-jet structure of the westerly winds in the Southern Hemisphere winter mesosphere. The gravity wave–resolving GCM of *Watanabe et al.* [2008] thus provides results for the first self-consistent numerical simulation of the eastward 4-day wave in the Antarctic winter mesosphere.

[6] In the present study, the eastward 4-day wave in the Antarctic winter mesosphere is characterized on the basis of this new GCM, and the relationships between the characteristics of the wave structures and the background mean flows are investigated in consideration of previous observational and theoretical studies, focusing on flow instabilities. As the 4-day wave develops from dynamically unstable flow structures, it is possible that the 4-day wave acts to stabilize the flow structures. The effects of the 4-day wave on the momentum budget in the middle of the mesospheric double-jet structure are investigated quantitatively by comparison with the contributions of the directly simulated small-scale gravity waves.

[7] Brief descriptions of the model and the period of analysis are given in section 2. Section 3.1 describes the seasonal marches of the zonal mean zonal wind and wave activities in the Southern Hemisphere winter stratosphere and mesosphere, focusing on wave mean flow interactions. Section 3.2 presents the results of a spatiotemporal Fourier analysis as the basis for determining the spectral filters to be used to extract the simulated 4-day wave. Section 3.3 describes the monthly mean activities of the 4-day waves, and examines the relationships between wave characteristics and flow instability. Section 3.4 discusses the evolution of the 4-day wave in terms of the $k = 1$ and $k = 2$ components, and section 3.5 investigates the dynamics of the 4-day wave in a number of characteristic wave events. Section 3.6 focuses on the roles of the 4-day wave in the zonal mean momentum

budget in the Antarctic winter mesosphere, and concluding remarks are provided in section 4.

2. Model Description

[8] The T213L256 middle atmosphere GCM developed for the KANTO project is employed in the present study [see *Watanabe et al.*, 2008]. The model has a horizontal triangularly truncated spectral resolution of T213, corresponding to a latitude–longitude grid interval of 0.5625° (62.5 km near the equator), and comprises 256 vertical layers from the surface to a height of approximately 85 km with a vertical resolution of 300 m throughout the middle atmosphere. No parameterization of subgrid gravity waves is used in the model in order to focus on the directly simulated gravity waves and their interactions with the large-scale circulations. Although the T213 horizontal resolution is insufficient to resolve very small gravity waves on the scale of 10 km, the vertical resolution is sufficiently fine to resolve the majority of observed gravity waves with acceptable accuracy [e.g., *Sato*, 1994; *Tsuda et al.*, 1994; *Allen and Vincent*, 1995; *Sato et al.*, 2003; *Sato and Yoshiki*, 2008]. In the model, gravity waves are spontaneously generated by a range of source mechanisms, including convection, topography, instability, and adjustment processes. The fine vertical resolution allows the model to accurately simulate the vertical propagation of gravity waves. The turbulent breakdown processes of gravity waves associated with shearing and convective instabilities cannot be directly represented by the model, and are instead represented by a Richardson number-dependent vertical diffusion parameterization in combination with dry convective adjustment. The monthly and zonal mean ozone climatology is prescribed in the model. The original ozone data set has the horizontal resolution of 2.5 by 2.5° in longitude and latitude and the vertical resolution of about 2 km in the stratosphere, extending from the surface to a 0.0011 hPa level (D. Li and K. P. Shine, UGAMP ozone climatology, British Atmospheric Data Center, 1999, available at http://badc.nerc.ac.uk/data/ugamp-o3-climatology/). We interpolated it into our model grid. A detailed description of the model and its characteristics for various simulated phenomena is given by *Watanabe et al.* [2008], *Tomikawa et al.* [2008], K. Sato et al. (On the origins of atmospheric gravity waves in the mesosphere, submitted to *Geophysical Research Letters*, 2009), Y. Kawatani et al. (The roles of equatorial trapped waves and three-dimensionally propagating gravity waves in driving the quasi-biennial oscillation. Part I: zonal mean wave forcing; Part II: Three-dimensional distribution of wave forcing, submitted to *Journal of the Atmospheric Sciences,* 2009), and K. Miyazaki et al. (Transport and mixing in the extratropical tropopause region in a high vertical resolution GCM. Part I: Potential vorticity and heat budget analysis, submitted to *Journal of the Atmospheric Sciences,* 2009).

[9] The GCM was executed for three successive years with a time step of 30 s, and it was confirmed that the seasonal march of the general circulation in the middle atmosphere was successfully reproduced throughout the simulation. In the present study, hourly sampled hourly mean data for the Antarctic winter months (June to September) in the first year

of the simulation are analyzed, during which the double-jet structure of mesospheric westerly winds often appears.

3. Results

3.1. Seasonal March of Mean Winds and Wave Forcing

[10] Figure 1 shows the monthly average zonal mean zonal wind and the Eliassen and Palm (EP) flux in the Southern Hemisphere upper stratosphere and mesosphere in June, July, August, and September. The EP flux and its divergence, representing wave forcing on the zonal mean zonal wind [e.g., *Andrews et al.*, 1987], are calculated separately for zonal wave numbers (k) of 1–5 (Figures 1b, 1e, 1h, and 1k) and >6 (Figures 1c, 1f, 1i, and 1l). The EP flux associated with the $k = 1$–5 wave components is mainly attributable to upward propagating planetary waves, while the latter ($k > 6$) is mainly due to upward propagating small-scale gravity waves with horizontal wavelengths of 200–1000 km [*Watanabe et al.*, 2008].

[11] The stratospheric polar night jet and the mesospheric subtropical jet are mixed in June and July. The westerly winds exhibit a single peak near 48°S, 0.3–0.5 hPa during this period. The activity of the upward propagating planetary waves is relatively weak, and the dissipation of these planetary waves creates a weak westward forcing on the equator side of the westerly jet.

[12] Strong enhancement of the upward propagating planetary waves occurs in August, causing a strong westward forcing near 40°S, 0.7 hPa. Such strong wave forcing results in separation of the stratospheric polar night jet from the mesospheric subtropical jet. The westward forcing due to upward propagating planetary waves shifts poleward and downward in August and September, in response to changes in the meridional structures of the polar vortex. In this period, the seasonal variation in the meridional structure of the stratospheric polar night jet appears to be driven by the upward propagating planetary waves in the stratosphere.

[13] In the middle and upper mesosphere, the meridional structure of the westerly winds including the subtropical jet stream is primarily maintained by westward forcing due to small-scale gravity waves. The stratospheric westerly winds extend to approximately 20°S in June and July. South of 20°S, small-scale gravity waves with westward intrinsic phase velocities, indicated by upward directed EP flux, propagate upward from the troposphere to the mesosphere. The dissipation of such westward propagating gravity waves creates westward forcing at the corresponding latitudes of the mesosphere. The westward forcing peaks at about 55°S in the upper mesosphere, and exhibits a triangular shape that is likely to influence the subtropical maximum of the mesospheric westerly winds and the secondary maximum of the mesospheric westerly winds near 70°S. This double-jet structure of the mesospheric westerly winds is of primary importance in reproducing excitation of the 4-day wave in the Antarctic winter mesosphere.

[14] The stratospheric polar night jet separates from the mesospheric subtropical jet in August and September. The westward propagating gravity waves only propagate upward within the stratospheric westerly winds and are thus confined to higher latitudes compared to those in June and July. The westward forcing due to gravity waves weakens and shifts poleward and downward in August and September, resulting

in the development of the double-jet structure in the Antarctic mesosphere above the stratospheric polar night jet.

[15] An interesting finding in Figure 1 is the eastward forcing due to planetary-scale ($k = 1$–5) waves appearing near the double-jet structure of the westerly winds in the Antarctic mesosphere (Figures 1b, 1e, 1h, and 1k), which offsets part of the westward forcing due to small-scale gravity waves (Figures 1c, 1f, 1i, and 1l). Such an effect modifies the meridional distribution of the total wave forcing in the polar mesosphere, and likely weakens the double-jet structure. The dynamics of the planetary-scale waves providing this eastward wave forcing are investigated in detail below.

3.2. Spectral Analysis

[16] The type of planetary-scale waves dominating the Antarctic winter mesosphere is investigated by spatiotemporal Fourier analysis [e.g., *Hayashi*, 1971]. Figure 2 shows zonal wave number–frequency spectra for a geopotential height of 0.1 hPa, calculated using hourly data for each month and averaged between 60°S and 70°S. The most prominent peaks occur in June and September in association with eastward $k = 1$ waves with periods longer than 10 days. These peaks are associated with quasi-stationary planetary waves, which are not considered in detail in the present study. The second largest peak occurs in July, and is associated with eastward $k = 2$ waves with a period of about 1.5 days. Similar but weaker peaks with slightly longer and shorter periods appear in June and August, respectively. The third largest peak, which occurs in August, is associated with eastward $k = 1$ waves with a period of about 3 days, and has a similar phase velocity to that of the $k = 2$ waves mentioned above. Weaker but similar peaks are apparent in June and September, with the latter having a period of approximately 4 days. These eastward $k = 1$ and $k = 2$ waves correspond to the 4-day wave of interest in the present study.

[17] The dynamics of the eastward $k = 1$ and $k = 2$ waves are examined by applying a spatiotemporal filter to the simulated three-dimensional velocity, temperature, and geopotential height fields. The band-pass periods adopted in the filter are determined such that wave components with the predominant periods of the simulated 4-day wave, that is, 3–4 days for the $k = 1$ wave and 1.3–1.7 days for the $k = 2$ wave, are successfully obtained. The $k = 1$ wave with periods of 2–4.5 days and the $k = 2$ wave with periods of 1.2–3 days are separately extracted using the filter, and the filtered data are considered in the analyses below.

3.3. Excitation of 4-Day Wave

[18] As an indicator of the necessary condition for dynamical instability in large-scale flow, the meridional gradient of the quasi-geostrophic potential vorticity ($\overline{q}_y$) is introduced, as defined by

$$\overline{q}_y \equiv \beta - \overline{u}_{yy} - \rho_0^{-1}\left(\rho_0 \frac{f^2}{N^2}\overline{u}_z\right)_z, \tag{1}$$

where β denotes the meridional derivative of the Coriolis parameter (f), $\overline{u}_{yy}$ denotes the meridional curvature of the zonal mean zonal wind in spherical coordinates [e.g., *Andrews et al.*, 1987], ρ_0 denotes density, N denotes the Brunt-Väisälä frequency, and subscript z denotes the vertical derivative. The possibility of flow instability is indicated by
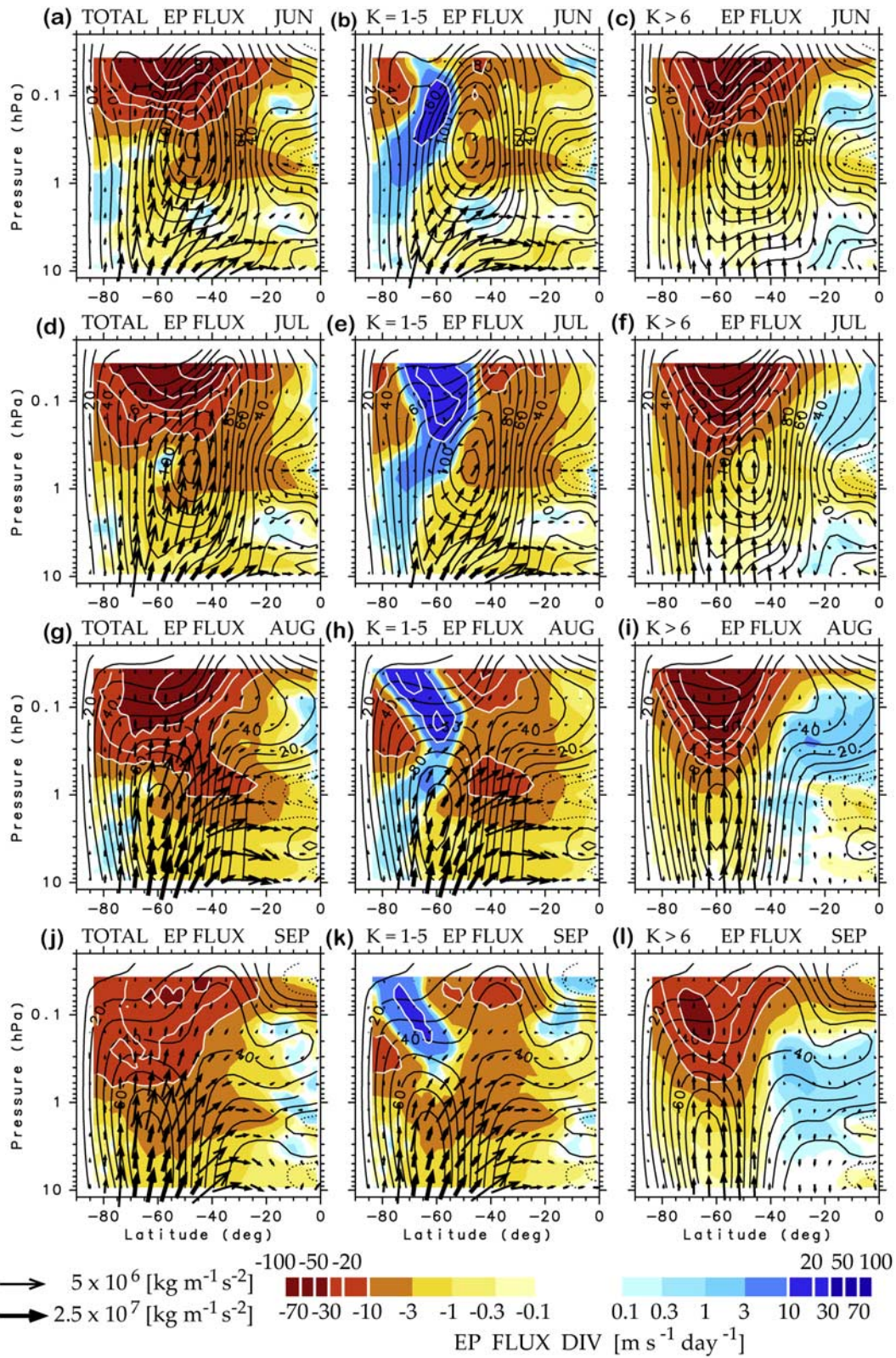
Figure 1. EP flux vectors (arrows) and eastward accelerations of zonal mean zonal wind due to divergence of EP flux (color scale) for (a–c) June, (d–f) July, (g–i) August, and (j–l) September (average). Figures 1a, 1d, 1g, and 1j are for total wave components. Figures 1b, 1e, 1h, and 1k are for $k = 1-5$. Figures 1c, 1f, 1i, and 1l are for $k > 6$. Vertical component of EP flux is multiplied by 220. Scale of arrows is altered for clarity, and color scale is logarithmic. Contours denote zonal mean zonal wind in 10 m s^{-1} intervals.
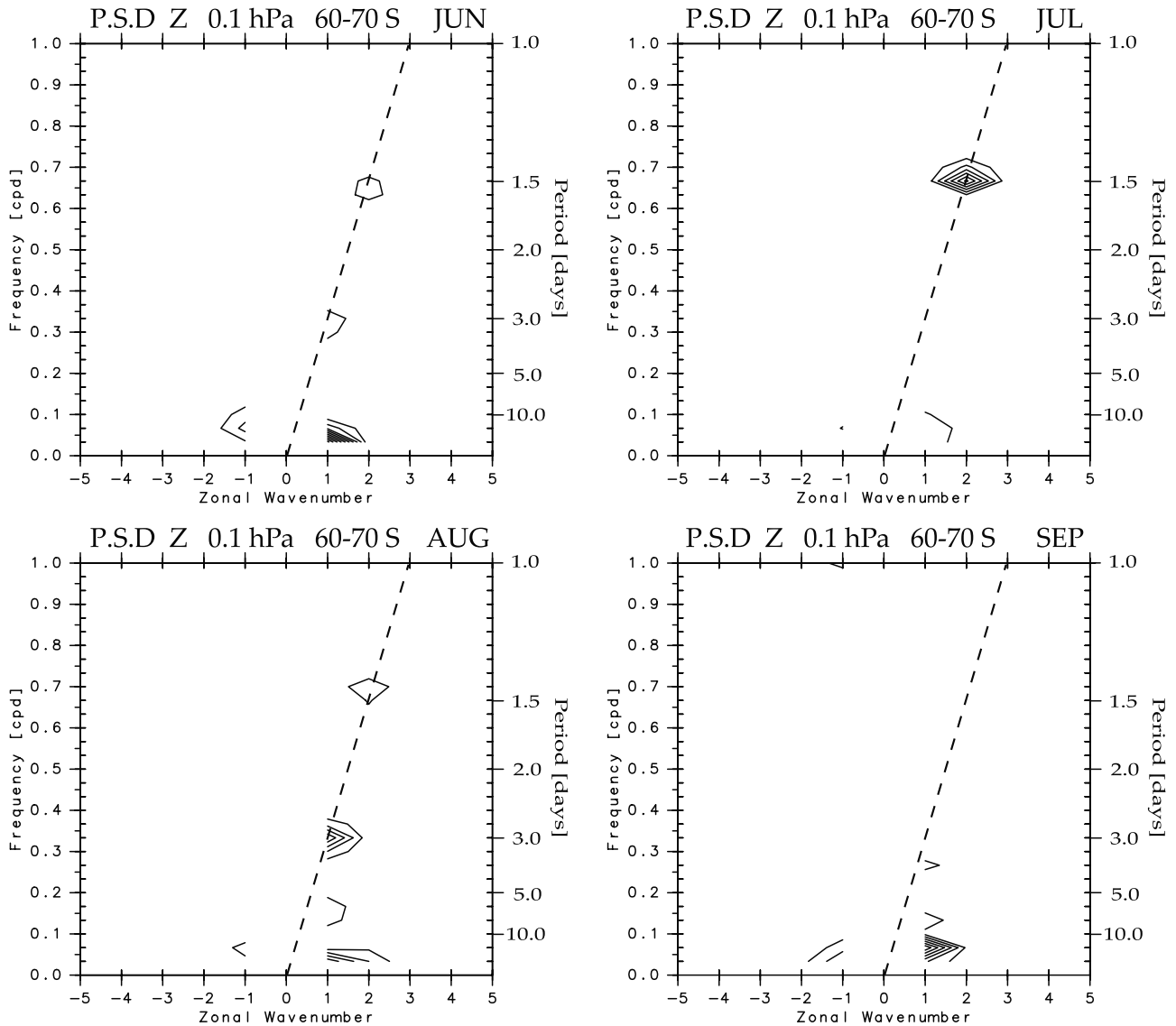
Figure 2. Zonal wave number versus frequency spectra at 0.1 hPa geopotential height averaged over $60-70°$S. Contour lines denote power spectral density in 300 m^2 d intervals. Positive (negative) zonal wave numbers indicate eastward (westward) traveling component relative to ground. Dashed line denotes ground-based eastward phase speed of 65.2 m s^{-1} at 65°S.

negative $\overline{q}_y$. As shown in Figure 3, negative $\overline{q}_y$ ($<-2 \times 10^{11}$ m^{-1} s^{-1}) for the monthly averaged zonal mean zonal wind in the polar mesosphere occurs between June and September. The negative $\overline{q}_y$ peaks near the poleward flank of the mesospheric jet in June and July, corresponding to strongly positive $\overline{u}_{yy}$. According to the analysis of wave forcing on the zonal mean zonal wind in section 3.1, the positive $\overline{u}_{yy}$ is maintained by gravity wave forcing, which rapidly strengthens with increasing latitude near the poleward flank of the westerly jet (Figures 1c, 1f, 1i, and 1l). In August and September, the negative $\overline{q}_y$ peaks in the middle of the double-jet structure above the stratospheric polar night jet, where the third term on the right-hand side of equation (1) becomes strongly negative because of the positive vertical curvature of the zonal mean zonal wind. Such a wind distribution is also maintained by the gravity wave forcing, described in section 3.1 (Figures 1c, 1f, 1i, and 1l).

[19] Figure 3 also shows the monthly mean distributions of the amplitude of geopotential height associated with the filtered 4-day wave, summed for the $k = 1$ and $k = 2$ waves (Figures 3a–3d). The geopotential height amplitude of the 4-day wave peaks in the vicinity of the negative $\overline{q}_y$ peak, and is distributed inside the polar vortex. In July and August, the maximal amplitude of the 4-day wave is sandwiched by negative and positive $\overline{q}_y$. The sign of $\overline{q}_y$ changes near the locations of the maximal geopotential height amplitude, near 63°S, 0.2 hPa in July and near 70°S, 0.15 hPa in August. At these locations, the zonal mean eastward wind speeds are approximately +70 m s^{-1} and +55 m s^{-1}, similar to the eastward phase speeds of the simulated 4-day wave (with period close to 3 days). Such relationships are expected if the simulated 4-day wave is advected by the mean winds at these locations [e.g., *Manney*, 1991].
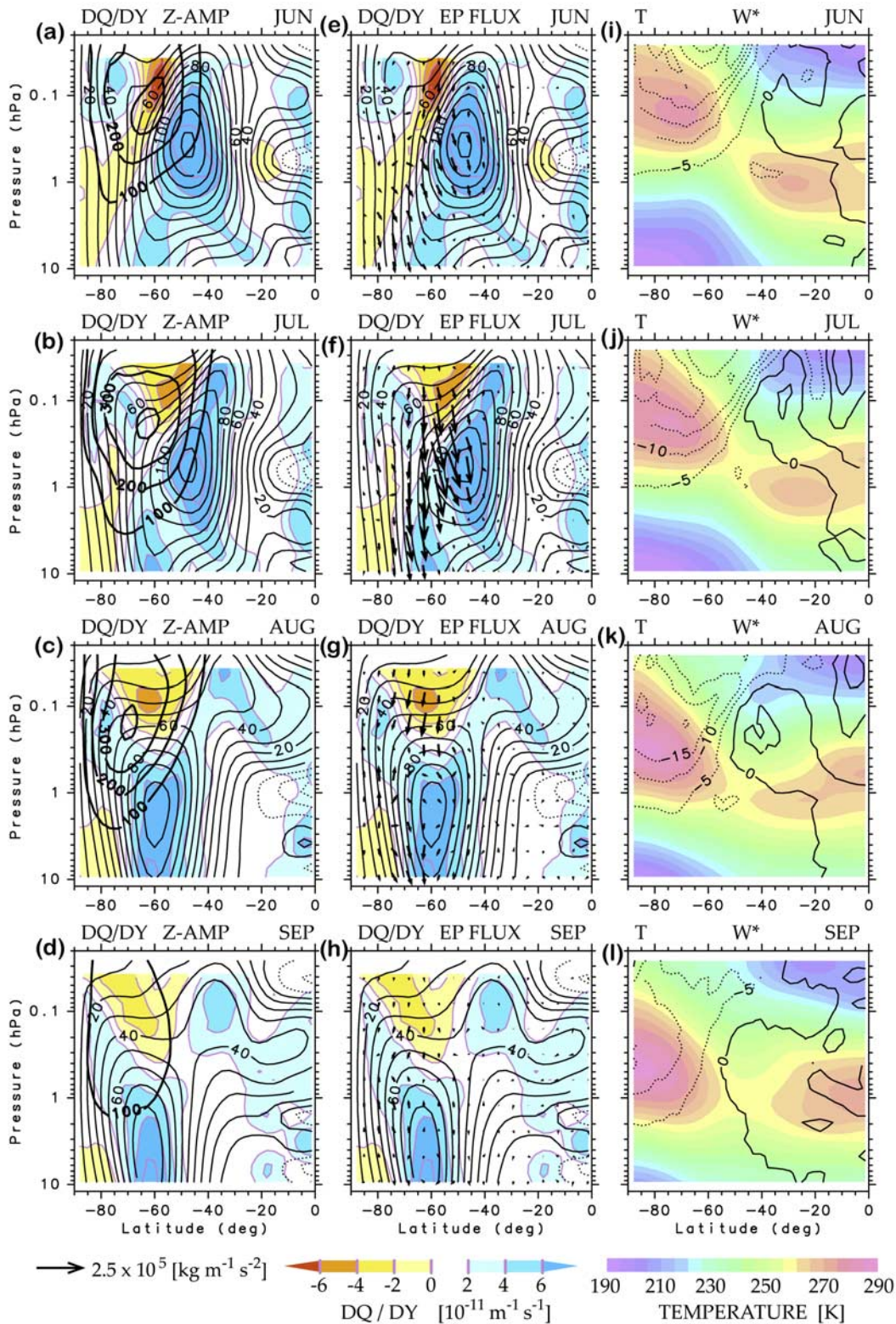
Figure 3. (a–d) Amplitude of geopotential height for filtered 4-day wave (bold contours, 100 m intervals) and zonal mean zonal wind (thin contours, 10 m s^{-1} intervals). (e–h) EP flux vectors (arrows) for filtered 4-day wave. Vertical component of EP flux is multiplied by 220 (scale of arrows differs from Figure 1). Color scale in Figures 3a–3h denotes meridional gradient of quasi-geostrophic potential vorticity ($\overline{q}_y$). (i–l) Residual mean vertical velocity (contours, 5 mm s^{-1} intervals) and zonal mean temperatures (color scale).

[20] The EP flux for the filtered waves (Figures 3e–3h) is directed downward and equatorward in June and July, from regions of negative $\overline{q}_y$ to regions of positive $\overline{q}_y$. Such distributions of EP flux strongly suggest that these waves develop from the mixed baroclinic and barotropic instabilities in the large-scale zonal flows, consistent with the widely accepted generation mechanism for the 4-day wave [e.g., *Manney and Randel*, 1993]. In August and September, the EP flux in the polar mesosphere is predominantly directed downward, likely indicating that baroclinic instability is prevalent in this period. The EP flux is strongest in July near the poleward flank of the polar night jet, and thereafter becomes significantly weaker, probably in association with the seasonal march of the mean flow structures.

[21] The simulated 4-day waves in the Antarctic mesosphere exhibit substantial equatorward heat flux, indicating the transport of heat from the warmer polar region to the colder subtropical mesosphere. The monthly averaged zonal mean temperatures in Figures 3i–3l reveal a distinct winter stratopause associated with the temperature maximum in the polar region, attributable to the descending motion induced by primarily gravity wave forcing (Figures 1c, 1f, 1i, and 1l). The residual mean vertical velocities [e.g., *Andrews et al.*, 1987] indicate strong descending motions in the mesosphere, raising temperatures in the polar region, and weak ascending motions producing lower temperatures in the subtropics. The resultant strong meridional gradient in mean temperature appears to be an important necessary condition for the occurrence of baroclinic instability in the Antarctic winter mesosphere.

3.4. Evolution of 4-Day Wave

[22] Figure 4 compares the evolution of the daily averaged zonal mean eastward wind at 0.1 hPa with the regions of negative $\overline{q}_y$. The mesospheric westerly jet peaks at 40–50°S, 0.1 hPa in association with the stratospheric polar night jet in June and July (see Figures 3a–3d for the monthly mean meridional cross sections). The mesospheric jet separates from the polar night jet as a result of strong wave forcing due to the upward propagating planetary waves in early August (not shown), accompanied by a decrease in wind speed from 80 to 100 m s^{-1} to 40–60 m s^{-1} (see also Figures 3a–3d). The negative $\overline{q}_y$ region occurs at 50–70°S throughout the analysis period. Westward forcing due to $k > 6$ waves is also apparent (Figure 4a), and is mainly attributable to small-scale gravity waves. The latitudinal distribution and day-to-day variation of gravity wave forcing are in very good agreement with those for negative $\overline{q}_y$, representing strong evidence that gravity wave forcing is a primary source mechanism for the large-scale flow instability in the Antarctic winter mesosphere.

[23] The amplitudes of geopotential height associated with the $k = 1$ and $k = 2$ waves, which have the predominant periods of 3–4 days and 1.3–1.7 days, respectively, are also shown in Figure 4. As pointed out above, the amplitudes of the simulated 4-day wave are confined to within the mesospheric westerly jet. Each 4-day wave event occurs in association with strongly negative $\overline{q}_y$, and persists for 10–20 days. The mature periods for the $k = 1$ and $k = 2$ wave events are largely exclusive, except for one event in mid-August referred to as event A. The EP flux divergence due to $k = 1$ and $k = 2$ waves (Figure 4) indicates that wave forcing due to the $k = 1$ wave is generally less pronounced than that associated with the $k = 2$ wave. The largest eastward wave forcing, exceeding +25 m s^{-1} d^{-1}, occurs at the beginning of July, corresponding to a growth period of $k = 2$ wave amplitude. The second largest eastward wave forcing (approximately +20 m s^{-1} d^{-1}) occurs in mid-July, corresponding to a mature period for the $k = 2$ wave (referred to as event J). The strongest amplification of the $k = 1$ wave occurs in event A, during which the eastward forcing of the $k = 1$ wave exceeds +15 m s^{-1} d^{-1}. Note that the eastward forcing due to the 4-day wave generally occurs in association with strongly negative $\overline{q}_y$. It is also noteworthy that westward forcing due to the 4-day wave sometimes occurs south of the eastward forcing, such as during event A, creating a north–south dipole structure. The wave events mentioned above, as highlighted in Figure 4, are investigated in more detail in section 3.5.

3.5. Wave Structures
3.5.1. Single-Jet Event in Mid-July

[24] Figure 5 shows the meridional distributions of $\overline{u}$ and $\overline{q}_y$, and the EP flux and divergence associated with the filtered 4-day waves during the typical wave events highlighted in Figure 4. During the strong $k = 2$ wave event in mid-July (event J), the zonal mean zonal winds describe a single-jet structure, and a region of strongly negative $\overline{q}_y$ ($<-6 \times 10^{-11}$ m^{-1} s^{-1}) exists near the poleward flank of the westerly jet in the upper mesosphere. A group of equatorward and downward directed EP flux vectors diverges near the negative $\overline{q}_y$ region, crossing the $\overline{q}_y$ contours and converges near the region of maximum positive $\overline{q}_y$ in the vicinity of the polar night jet. The divergence of EP flux causes eastward wave forcing on the zonal mean westerly winds of more than +10 m s^{-1} d^{-1} near the region of negative $\overline{q}_y$, probably contributing to a weakening of the negative $\overline{q}_y$ and thus stabilizing the large-scale flow. The convergence of EP flux near the center of the polar night jet causes only weak westward forcing because of the increase in atmospheric density.

[25] Figure 6 shows a series of synoptic maps of geopotential height and temperature at 0.1 hPa during one cycle of the $k = 2$ wave. Large-scale features of the zonal average and $k = 1-5$ component are also shown. The mesospheric subtropical jet or the edge of the polar vortex is located near 40°S (Figures 5a and 5d). Inside the polar vortex, the temperature generally increases with latitude. The dominance of a $k = 2$ wave pattern can be identified from the filtered geopotential height and temperature associated with the 4-day wave shown in Figure 6. As the $k = 2$ wave propagates eastward with a period of ~1.5 days, the elongated structure corresponding to the inner polar vortex rotates eastward. Superposition of the weak $k = 1$ temperature anomalies on the dominant $k = 2$ anomalies results in a weak cold pool (-3 to -6 K) that circulates above the coastline of Antarctica. The bending horizontal phase structure of the geopotential height disturbances coincides with the poleward transport of eastward momentum expressed by the equatorward EP flux (see Figures 5a and 5d). The phase relationships between the temperature and geopotential height anomalies indicate equatorward heat transport, in agreement with the downward EP flux.
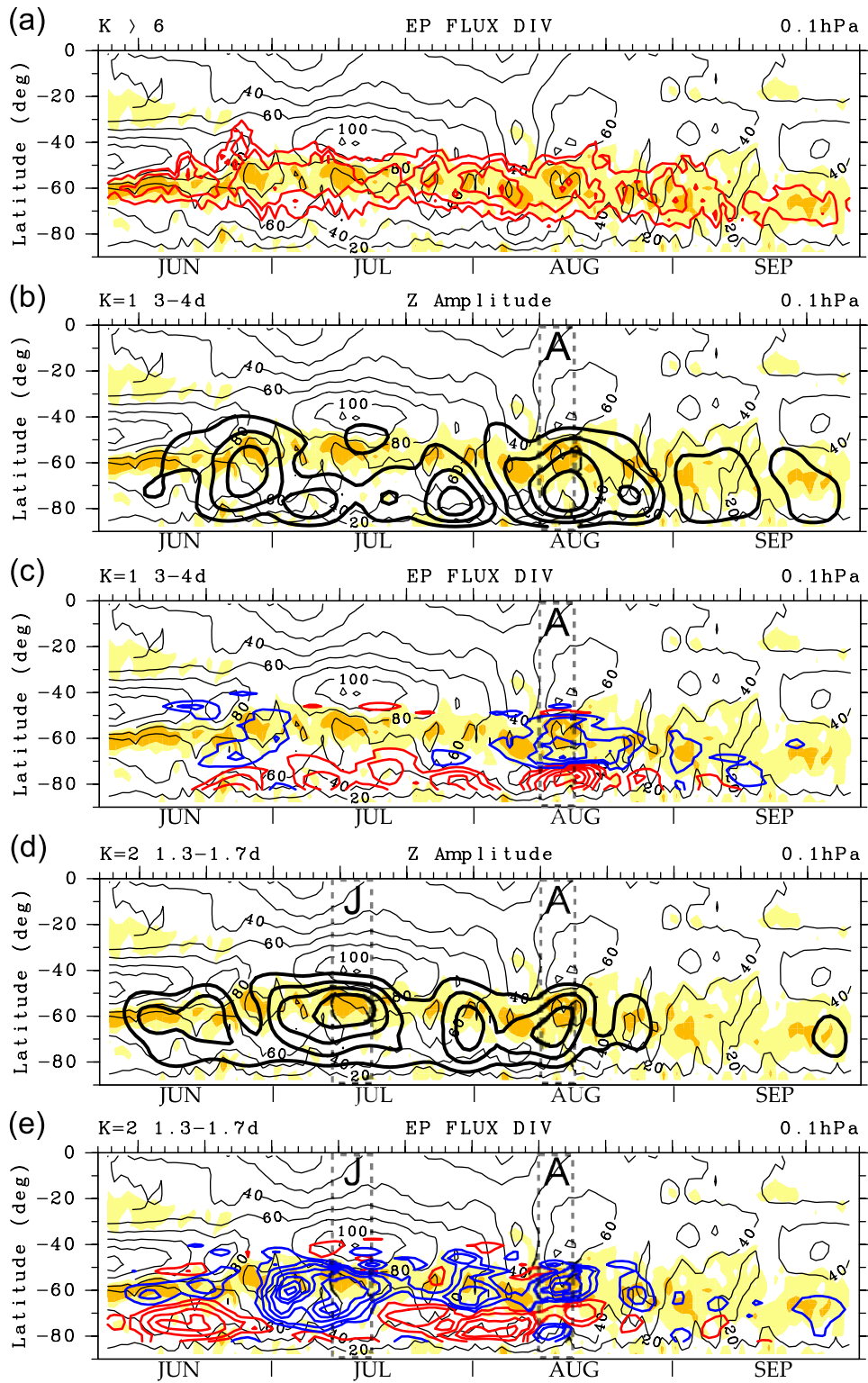
Figure 4. Latitude-time cross sections at 0.1 hPa. Thin contours denote zonal mean zonal winds (20 m s^{-1} intervals), yellow denotes regions of $\overline{q}_y < 0$, and orange denotes regions of $\overline{q}_y < -5 \times 10^{-11}$ m^{-1} s^{-1}. (a) Eastward forcing due to $k > 6$ waves (red contours at -30, -50, and -80 m s^{-1} d^{-1}). Amplitude of geopotential height for (b) $k = 1$ wave with period of $3-4$ days and (d) $k = 2$ wave with period of $1.3-1.7$ days (bold contours, 100 m intervals). Eastward forcing for filtered (c) $k = 1$ wave with period of $3-4$ days and (e) $k = 2$ wave with period of $1.3-1.7$ days (blue contours at $+2$, $+5$, $+10$, $+15$, $+20$, $+25$, and $+30$ m s^{-1} d^{-1}), and westward forcing (red contours at -2, -5, -10, -15, -20, -25, and -30 m s^{-1} d^{-1}). Daily averaged time series is displayed in Figure 4a, while 5-day running averaged values are displayed in Figures 4b–4e for clarity. J and A denote wave events mentioned in section 3.4.
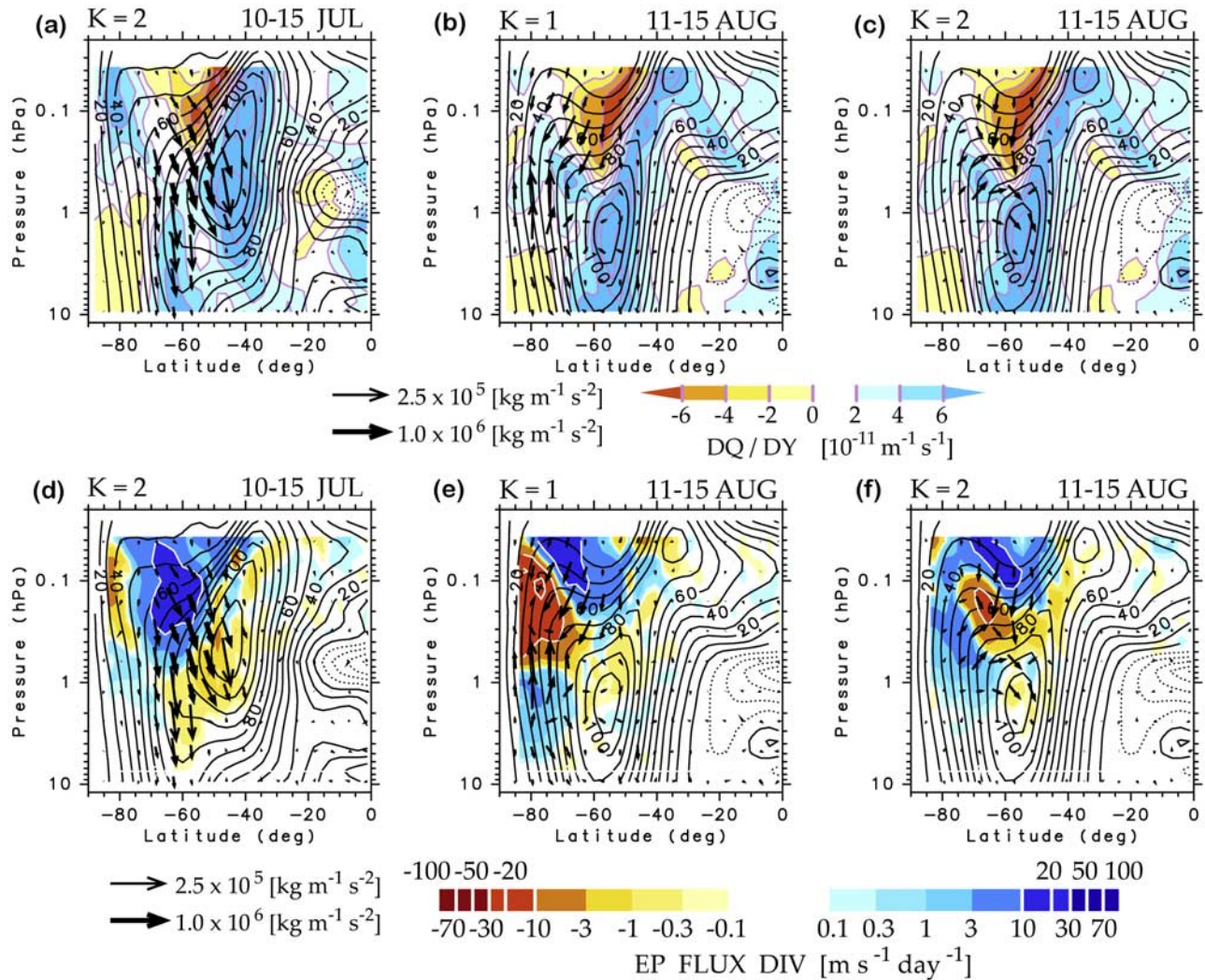
Figure 5. EP flux vectors (arrows) for filtered 4-day wave averaged for the period of each wave event. Vertical component of EP flux is multiplied by 220. Scale of arrows is altered for clarity. Contours denote zonal mean zonal wind in 10 m s^{-1} intervals. (a–c) Meridional gradient of quasi-geostrophic potential vorticity ($\bar{q}_y$, color scale). (d–f) Eastward acceleration of zonal mean zonal wind due to divergence of EP flux (logarithmic color scale).

3.5.2. Double-Jet Event in Mid-August

[26] The meridional distributions of $\bar{u}$ and $\bar{q}_y$, and the EP flux and divergence associated with the $k = 1$ and $k = 2$ waves during the wave event in mid-August (event A, Figure 4) are shown in Figures 5b, 5c, 5e, and 5f. This is a typical double-jet event, during which the negative $\bar{q}_y$ reaches a peak between the mesospheric subtropical jet and the secondary jet at $70–80°$S. This wind distribution resembles that derived from monthly averages of observed temperatures in August 1976 and 1977 [*Lawrence and Randel*, 1996], although the simulated westerly winds are stronger than those observed. A group of $k = 1$ EP flux vectors diverges in the polar half of the negative $\bar{q}_y$ region, directed poleward and downward, crossing $\bar{q}_y$ contours and converges near the regions of maximal positive $\bar{q}_y$ in the vicinity of the secondary jet. The divergence and convergence of $k = 1$ EP flux produce a dipole pattern sandwiching the peak of the secondary jet, causing the secondary jet to move equator-

ward. Another group of $k = 1$ EP flux vectors can also be observed, originating from the region of negative $\bar{q}_y$ on the poleward flank of the stratospheric polar night jet near $80°$S, 3 hPa. Some of the EP flux vectors are directed upward and converge in the Antarctic mesosphere, while others are directed equatorward and downward, converging near the stratospheric polar night jet. The dynamics of these stratospheric 4-day waves and the generation mechanism of the negative $\bar{q}_y$ region on the poleward flank of the stratospheric polar night jet are beyond the scope of the present study.

[27] The EP flux associated with the $k = 2$ wave can be seen in the middle of the double-jet structure, at lower latitudes compared with the $k = 1$ EP flux. The $k = 2$ EP flux is also directed poleward and downward, diverging from the maximal negative $\bar{q}_y$ between the two jets and converging near the top of the stratospheric polar night jet. The eastward wave forcing associated with the $k = 2$ wave is weaker and peaks at lower latitudes compared to the $k = 1$ wave, and the
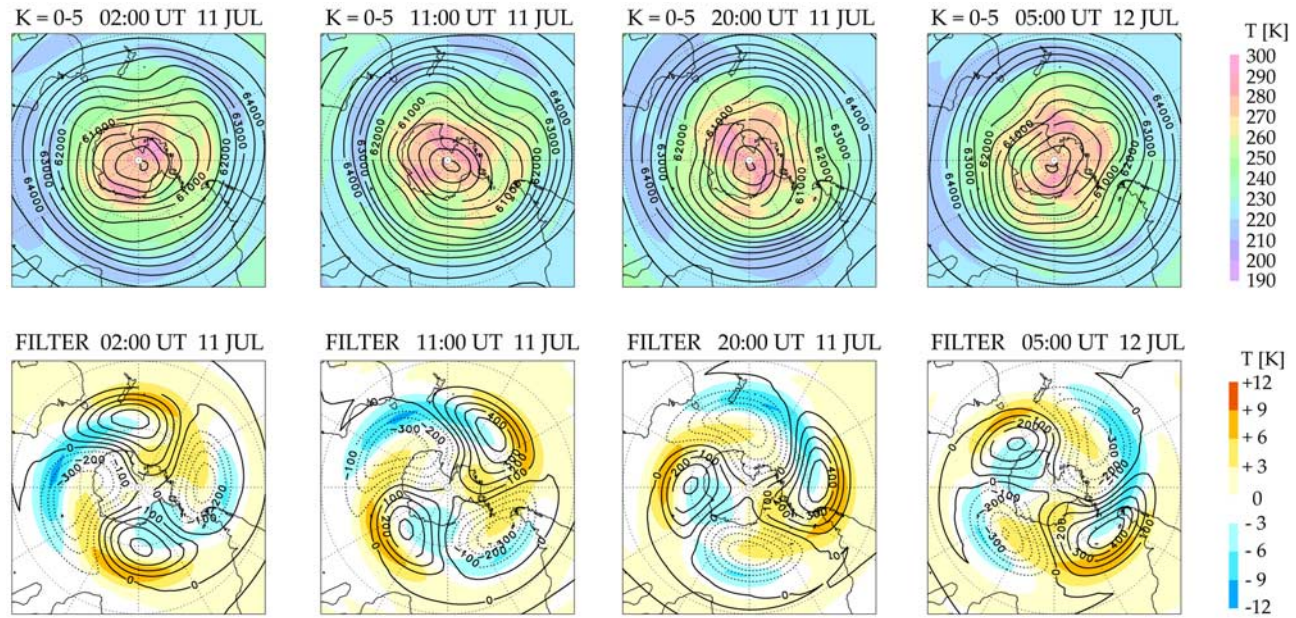
Figure 6. Series of synoptic maps showing geopotential height (contours) and temperatures (color scale) at 0.1 hPa during one cycle of the filtered $k = 2$ wave. (top) The $k = 0-5$ components with the contour interval of 500 m. (bottom) The filtered 4-day wave with the contour interval of 100 m. Dateline is located at the top, and the inner and outer latitude circles denote 60°S and 30°S, respectively.

sum of the two waves creates a broad eastward wave forcing that extends across the entire region around the double-jet structure.

[28] Figure 7 shows a series of synoptic maps of geopotential height and temperature at 0.1 hPa during one cycle of the $k = 1$ wave. Within the mesospheric subtropical jet, above Antarctica, the center of the polar vortex circles eastward around the South Pole following the low-pressure anomaly of the 4-day wave produced by the sum of the $k = 1$ and $k = 2$ waves. A distinct warm pool with a large temperature anomaly of +9 to +12 K also circles eastward around the South Pole above the Antarctic coastline, with a period of approximately 3 days. The phase relationships between the temperature and geopotential height anomalies indicate
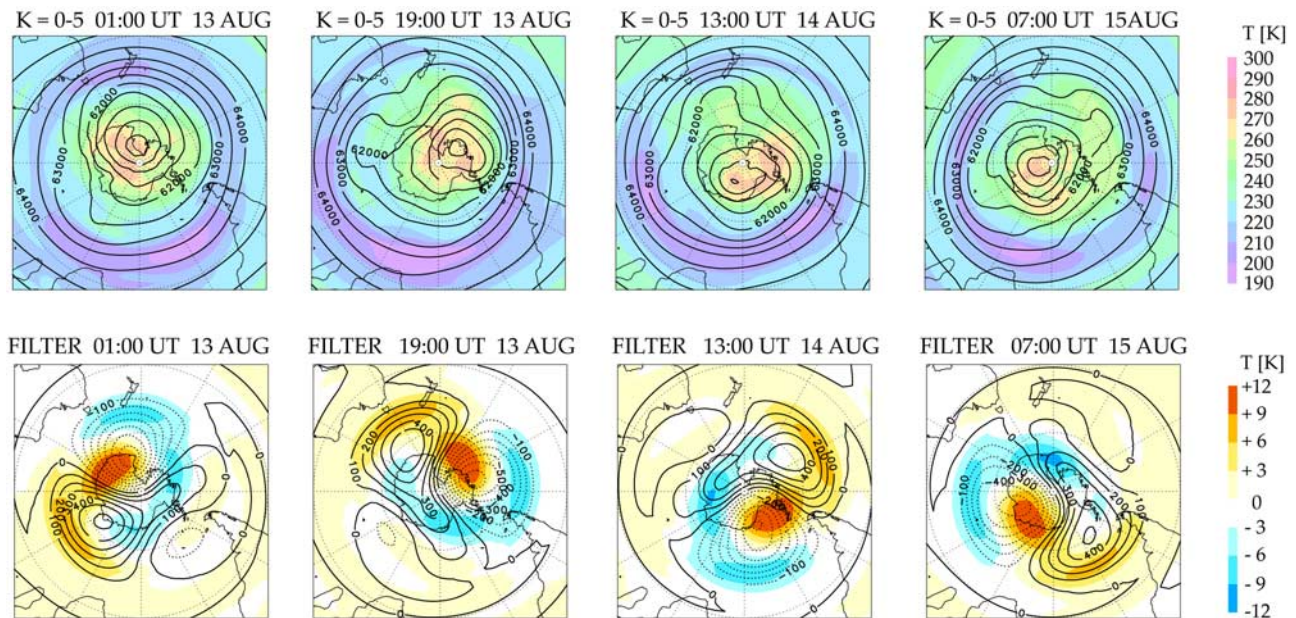
Figure 7. Series of synoptic maps for the $k = 1$ plus $k = 2$ wave event in mid-August showing geopotential height (contours) and temperatures (color scale) at 0.1 hPa during one cycle of the filtered $k = 1$ wave. (top) The $k = 0-5$ components with the contour interval of 500 m. (bottom) The filtered 4-day wave with the contour interval of 100 m. Dateline is located at the top, and the inner and outer latitude circles denote 60°S and 30°S, respectively.
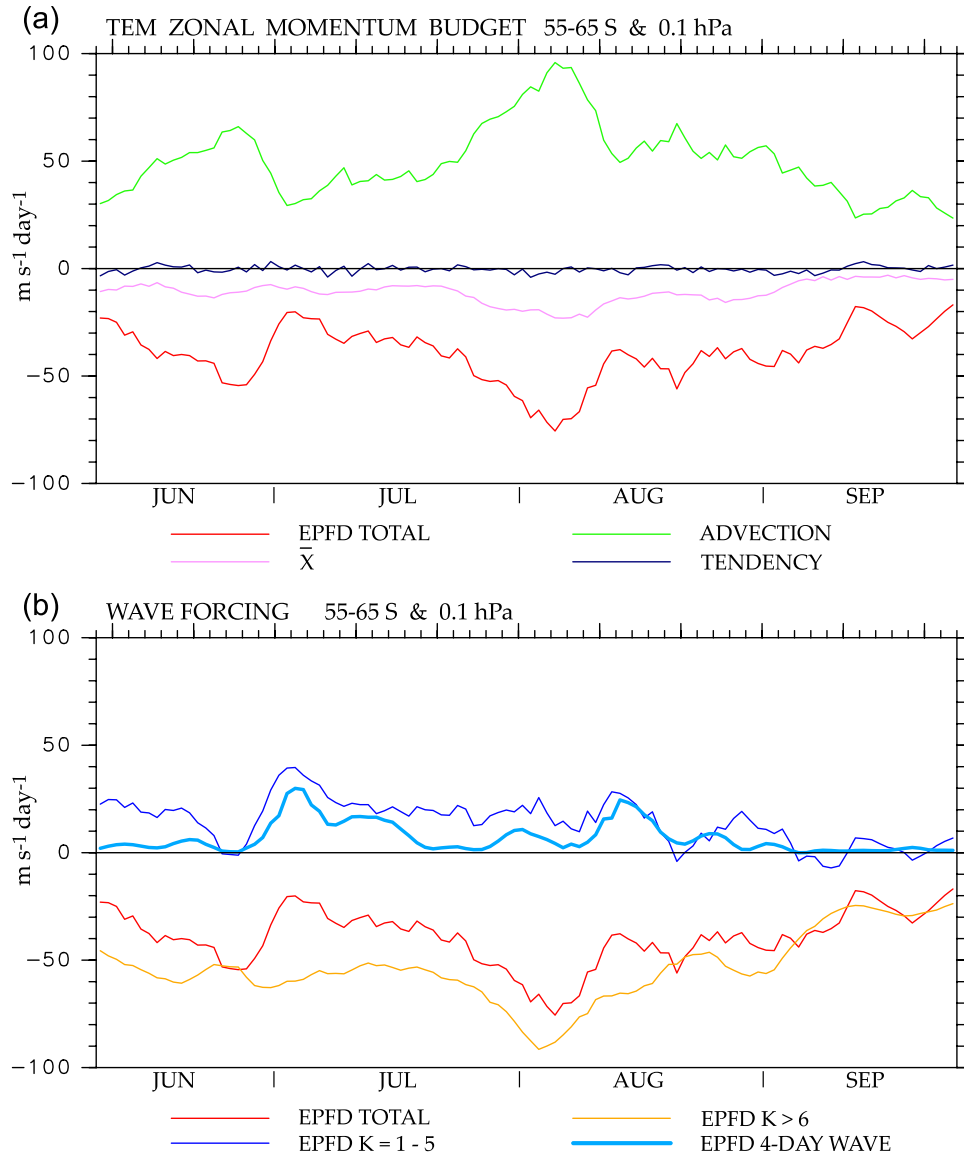
Figure 8. (a) The 5-day running mean time series for each term of the transformed Eulerian mean zonal momentum equation at 0.1 hPa averaged over $55-65°S$ (see section 3.6). EPFD denotes eastward wave forcing due to EP flux divergence. (b) Eastward wave forcing associated with each wave component.

strong equatorward heat transport corresponding to the downward EP flux (see Figures 5b, 5c, 5e, and 5f).

3.6. Effect of 4-Day Wave on Momentum Budget

[29] During the wave events described above, the eastward forcing due to the simulated 4-day wave acts to accelerate the zonal mean westerly winds ($\overline{u}$) near the negative $\overline{q}_y$ region in the Antarctic winter mesosphere, where gravity wave forcing causes strong deceleration of $\overline{u}$. The role of wave forcing due to the 4-day wave in the zonal momentum budget is quantified here in comparison with that associated with gravity waves. Figure 8 shows the evolution of each term of the transformed Eulerian mean zonal momentum equation, as given by [e.g., *Andrews et al.*, 1987]

$$\frac{\partial \overline{u}}{\partial t} = -(\overline{u}_y - f)\overline{v}^* - \frac{\partial \overline{u}}{\partial p}\overline{\omega}^* + \nabla \cdot F + \overline{X}. \quad (2)$$

These terms are calculated and averaged over the interval $55-65°S$ at 0.1 hPa, where the eastward forcing due to the 4-day wave reaches a maximum in July and August. The advection term in Figure 8 corresponds to the sum of the first and second terms on the right-hand side of equation (2), which include the residual mean meridional and pressure velocities ($\overline{v}^*$, $\overline{\omega}^*$). The divergence of EP flux ($\nabla \cdot F$) represents eastward zonal forcing due to the total wave component. The running average of 5 days is shown for each term. In these averaged time series, tendency of $\overline{u}$ becomes negligibly small, and the total wave forcing term (negative values) is roughly balanced with the advection term (positive values). The nonconservative term ($\overline{X}$) is calculated as the residual of the small-$\overline{u}$ tendency, advection, and the total wave forcing terms, and represents the effects of unresolved physical processes such as horizontal and vertical diffusion.

[30] The wave forcing calculated separately for the $k = 1-5$ and $k > 6$ components, and the filtered 4-day wave

components, are shown in Figure 8b. The total wave forcing is dominated by strong westward forcing due to the $k > 6$ component associated with the dissipation of gravity waves, and evolves slowly compared to the $k = 1-5$ component. The gravity wave forcing is approximately -60 m s^{-1} d^{-1} in June and July, increasing to approximately -100 m s^{-1} d^{-1} in early August and decreasing thereafter. Such westward forcing continuously generates negative $\overline{q}_y$ near the location of analysis (see Figures 1c, 1f, 1i, 1l, 3a–3d, and 4), leading to generation of the 4-day waves. The eastward forcing due to the 4-day wave occupies much of the $k = 1-5$ component in July and August, and significantly alters the evolution of the total wave forcing. During the strongest event at the beginning of July, the eastward forcing due to the 4-day wave offsets more than half of the westward gravity wave forcing, resulting in a weakening of the total westward wave forcing. A contemporaneous decrease in the advection term is seen in Figure 8, probably resulting from a decrease in poleward flows induced by the total wave forcing. A weaker but similar enhancement of eastward forcing due to the 4-day wave is apparent on some occasions, weakening the total wave forcing and the meridional circulation with a time scale of $10-20$ days.

4. Concluding Remarks

[31] The characteristics of the eastward 4-day wave in the Antarctic winter mesosphere simulated using the T213L256 middle atmosphere GCM were analyzed and compared with the seasonal march of the meridional structures of the westerly jet streams in the Southern Hemisphere upper stratosphere and mesosphere. It was found that the $k = 1$ and $k = 2$ components of the 4-day wave have periods of $3-4$ days and $1.3-1.7$ days, respectively, with eastward phase speeds consistent with the wind speeds of the eastward mean flows near the maximal geopotential height amplitude of the waves, where $\overline{q}_y$ changes sign. The 4-day wave was shown to develop near regions of negative $\overline{q}_y$ either near the poleward flank of the mesospheric subtropical jet or between the two jets of the double-jet structure of the mesospheric westerly winds, where westward forcing due to gravity waves creates strongly positive curvature of $\overline{u}$. The EP flux was found to diverge near the region of maximal negative $\overline{q}_y$ and to converge near the region of positive $\overline{q}_y$ associated with maximal $\overline{u}$. Such effects likely act to reduce the negative $\overline{q}_y$ value. The $k = 2$ component was dominant in July, creating an elongated inner polar vortex that circles eastward above Antarctica with a period of $\sim$1.5 days, while a mixed $k = 1$ and $k = 2$ wave event occurred in mid-August, creating strong warm pool of $+9$ to $+12$ K that circles eastward near the Antarctic coast line with a period of $\sim$3 days. The eastward forcing due to the 4-day wave was found to have a substantial impact on the zonal mean momentum budget in the Antarctic winter mesosphere, offsetting part of the westward forcing due to gravity waves and creating intraseasonal variation in the total wave forcing with a time scale of $10-20$ days. These characteristics suggest that the eastward 4-day wave in the Antarctic winter mesosphere is essentially a mixed baroclinic and barotropic wave that develops in the large-scale mean flow under strong distortion by gravity wave forcing. The gravity wave forcing causes not only distortion of the mesospheric westerly winds

(e.g., forming a double-jet structure), but also strong baroclinicity in the Antarctic winter mesosphere by driving poleward meridional overturning circulation, the descending motion of which raises temperatures in the polar cap region while the ascending motion lowers temperatures at the subtropics.

[32] The overall findings in the present study support previous observational and theoretical studies [e.g., *Randel and Lait*, 1991; *Lawrence and Randel*, 1996; *Manney and Randel*, 1993]. *Randel and Lait* [1991] analyzed observational temperature data for the stratosphere in August 1980, and resolved 4-day wave EP flux vectors directed downward and equatorward near $50-60°$S at the stratopause. It was suggested that flow instability associated with the mesospheric double-jet structure might be the origin of the observed 4-day wave, which is supported by the present simulation. The evolution of the 4-day wave at 1 hPa derived in that study is also generally similar to that at 0.1 hPa described in the present study (Figure 4). *Manney and Randel* [1993] later conducted stability calculations using the climatological zonal mean zonal winds in August, and concluded that both baroclinic and barotropic instabilities associated with the double-jet structure in the mesosphere were necessary to realize rapid growth of the 4-day wave. *Lawrence and Randel* [1996] reported another type of 4-day wave that developed in the Antarctic mesosphere in September 1977 associated with flow instability between the stratospheric polar night jet and the mesospheric subtropical jet. However, the mean flow distribution and wave characteristics of that event differ from those reported in the present study. The present study provides valuable insights on the variety of 4-day wave characteristics associated with the background conditions in the Antarctic winter mesosphere, where the number of observational and numerical studies remains limited compared to those for the stratosphere.

[33] The most interesting finding in the present study is the influence of the 4-day wave on the momentum budget. As detailed analysis of the zonal momentum budget accounting for gravity wave forcing cannot be performed using existing observational data sets, this result provides new and valuable information. The 4-day wave develops in baroclinically and barotropically unstable flow originally caused by gravity wave forcing, and it is thus natural that the 4-day wave acts against gravity wave forcing as found in the present study. Groups of small-scale gravity waves generated in the troposphere propagate through the mean westerly winds of the polar vortex, and the dissipation of those gravity waves results in strong localized friction with the mesospheric westerly winds, distorting the mean flow to create regions of negative $\overline{q}_y$. The planetary-scale 4-day wave generated by the flow instability moves eastward with the mean westerly winds within the mesospheric polar vortex, and the resulting transport of momentum and heat acts to accelerate the mean westerly winds near the negative $\overline{q}_y$ region. Although the wave forcing due to the 4-day wave is weaker than that due to gravity waves, the 4-day wave is the primary dynamic mechanism that acts to partially stabilize the unstable mean flow structure in the Antarctic winter mesosphere caused by gravity wave forcing, leading toward dynamically stable conditions.

[34] The origins and propagation of gravity waves in the Antarctic winter mesosphere simulated by the high-resolution

GCM have been discussed by *Watanabe et al.* [2006, 2008] and *Watanabe* [2008], and further details will be given in a forthcoming paper by Sato et al. (submitted manuscript, 2009). More comprehensive analyses on the seasonal march of the extratropical general circulation in the present GCM simulation are currently planned, and the roles of various kinds of atmospheric waves in the zonal mean momentum budget will be elucidated in the near future. The detailed sequence of growth of the 4-day wave may also be investigated separately in the future.

References

Alexander, M. J., and C. Barnet (2007), Using satellite observations to constrain parameterizations of gravity wave effects for global models, *J. Atmos. Sci.*, *64*, 1652–1665, doi:10.1175/JAS3897.1.

Alexander, M. J., et al. (2008), Global estimates of gravity wave momentum flux from High Resolution Dynamics Limb Sounder observations, *J. Geophys. Res.*, *113*, D15S18, doi:10.1029/2007JD008807.

Allen, D. R., J. L. Stanford, L. S. Elson, E. F. Fishbein, L. Froidevaux, and J. W. Waters (1997), The 4-day wave as observed from the Upper Atmosphere Research Satellite Microwave Limb Sounder, *J. Atmos. Sci.*, *54*, 420–434, doi:10.1175/1520-0469(1997)054<0420:TDWAOF>2.0.CO;2.

Allen, S. J., and R. A. Vincent (1995), Gravity wave activity in the lower atmosphere: Seasonal and latitudinal variations, *J. Geophys. Res.*, *100*, 1327–1350, doi:10.1029/94JD02688.

Andrews, D. G., J. R. Holton, and C. B. Leovy (1987), *Middle Atmosphere Dynamics*, 489 pp., Academic, San Diego, Calif.

Ern, M., P. Preusse, M. J. Alexander, and C. D. Warner (2004), Absolute values of gravity wave momentum flux derived from satellite data, *J. Geophys. Res.*, *109*, D20103, doi:10.1029/2004JD004752.

Ern, M., P. Preusse, and C. D. Warner (2006), Some experimental constraints for spectral parameters used in the Warner and McIntyre gravity wave parameterization scheme, *Atmos. Chem. Phys.*, *6*, 4361–4381.

Fritts, D. C., and M. J. Alexander (2003), Gravity wave dynamics and effects in the middle atmosphere, *Rev. Geophys.*, *41*(1), 1003, doi:10.1029/2001RG000106.

Garcia, R. R., R. Lieberman, J. M. Russell III, and M. G. Mlynczak (2005), Large-scale waves in the mesosphere and lower. thermosphere observed by SABER, *J. Atmos. Sci.*, *62*, 4384–4399, doi:10.1175/JAS3612.1.

Hartmann, D. L. (1983), Barotropic instability of the polar night jet stream, *J. Atmos. Sci.*, *40*, 817–835, doi:10.1175/1520-0469(1983)040<0817:BIOTPN>2.0.CO;2.

Hayashi, Y. (1971), A generalized method of resolving disturbances into progressive and retrogressive waves by space Fourier and time cross-spectral analyses, *J. Meteorol. Soc. Jpn.*, *49*, 125–128.

Lait, L., and J. Stanford (1988), Fast, long-lived features in the polar stratosphere, *J. Atmos. Sci.*, *45*, 3800–3809, doi:10.1175/1520-0469(1988)045<3800:FLLFIT>2.0.CO;2.

Lawrence, B. N., and W. J. Randel (1996), Variability in the mesosphere observed by the Nimbus6 pressure modulator radiometer, *J. Geophys. Res.*, *101*(D18), 23,475–23,489, doi:10.1029/96JD01652.

Lawrence, B. N., G. J. Fraser, R. A. Vincent, and A. Phillips (1995), The 4-day wave in the Antarctic mesosphere, *J. Geophys. Res.*, *100*, 18,899–18,908, doi:10.1029/95JD01168.

Manney, G. L. (1991), The stratospheric 4-day wave in NMC data, *J. Atmos. Sci.*, *48*, 1798–1811, doi:10.1175/1520-0469(1991)048<1798:TSDWIN>2.0.CO;2.

Manney, G. L., and W. J. Randel (1993), Instability at the winter stratopause: A mechanism for the 4-day wave, *J. Atmos. Sci.*, *50*, 3928–3938, doi:10.1175/1520-0469(1993)050<3928:IATWSA>2.0.CO;2.

Manney, G. L., T. R. Nathan, and J. L. Stanford (1988), Barotropic stability of realistic stratospheric jets, *J. Atmos. Sci.*, *45*, 2545–2555, doi:10.1175/1520-0469(1988)045<2545:BSORSJ>2.0.CO;2.

Manney, G. L., Y. J. Orsolini, H. C. Pumphrey, and A. E. Roche (1998), The 4-day wave and transport of UARS tracers in the austral polar vortex, *J. Atmos. Sci.*, *55*, 3456–3470, doi:10.1175/1520-0469(1998)055<3456:TDWATO>2.0.CO;2.

McLandress, C. (1998), On the importance of gravity waves in the middle atmosphere and their parameterization in general circulation models, *J. Atmos. Sol. Terr. Phys.*, *60*, 1357–1383, doi:10.1016/S1364-6826(98)00061-3.

McLandress, C., and J. F. Scinocca (2005), The GCM response to current parameterizations of non-orographic gravity wave drag, *J. Atmos. Sci.*, *62*, 2394–2413, doi:10.1175/JAS3483.1.

Merzlyakov, E. G., and D. V. Pancheva (2007), The 1.5–5 day eastward waves in the upper stratosphere-mesosphere as observed by the Esrange meteor radar and the SABER instrument, *J. Atmos. Sol. Terr. Phys.*, *69*, 2102–2117, doi:10.1016/j.jastp.2007.07.002.

Prata, A. J. (1984), The 4-day wave, *J. Atmos. Sci.*, *41*, 150–155, doi:10.1175/1520-0469(1984)041<0150:TDW>2.0.CO;2.

Preusse, P., et al. (2006), Tropopause to mesopause gravity waves in August: Measurement and modeling, *J. Atmos. Sol. Terr. Phys.*, *68*, 1730–1751, doi:10.1016/j.jastp.2005.10.019.

Preusse, P., S. D. Eckermann, M. Ern, J. Oberheide, R. H. Picard, R. G. Roble, M. Riese, J. M. Russell III, and M. G. Mlynczak (2009), Global ray tracing simulations of the SABER gravity wave climatology, *J. Geophys. Res.*, *114*, D08126, doi:10.1029/2008JD011214.

Randel, W. J., and L. R. Lait (1991), Dynamics of the 4-day wave in the Southern Hemisphere polar stratosphere, *J. Atmos. Sci.*, *48*, 2496–2508, doi:10.1175/1520-0469(1991)048<2496:DOTDWI>2.0.CO;2.

Sato, K. (1994), A statistical study of the structure, saturation and sources of inertio-gravity waves in the lower stratosphere observed with the MU radar, *J. Atmos. Terr. Phys.*, *56*, 755–774, doi:10.1016/0021-9169(94)90131-7.

Sato, K., and M. Yoshiki (2008), Gravity wave generation around the polar vortex in the stratosphere revealed by 3-hourly radiosonde observations at Syowa Station, *J. Atmos. Sci.*, *65*, 3719–3735, doi:10.1175/2008JAS2539.1.

Sato, K., M. Yamamori, S. Ogino, N. Takahashi, Y. Tomikawa, and T. Yamanouchi (2003), A meridional scan of the stratospheric gravity wave field over the ocean in 2001 (MeSSO2001), *J. Geophys. Res.*, *108*(D16), 4491, doi:10.1029/2002JD003219.

Tomikawa, Y., K. Sato, S. Watanabe, Y. Kawatani, K. Miyazaki, and M. Takahashi (2008), Wintertime temperature maximum at the subtropical stratopause in a T213L256 GCM, *J. Geophys. Res.*, *113*, D17117, doi:10.1029/2008JD009786.

Tsuda, T., Y. Murayama, H. Wiryosumarto, S. W. B. Harijono, and S. Kato (1994), Radiosonde observations of equatorial atmosphere dynamics over Indonesia: 2. Characteristics of gravity waves, *J. Geophys. Res.*, *99*(D5), 10,507–10,516, doi:10.1029/94JD00354.

Venne, D. E., and J. L. Stanford (1979), Observation of a 4-day temperature wave in the polar winter stratosphere, *J. Atmos. Sci.*, *36*, 2016–2019, doi:10.1175/1520-0469(1979)036<2016:OOATWI>2.0.CO;2.

Venne, D. E., and J. L. Stanford (1982), An observational study of high-latitude stratospheric planetary waves in winter, *J. Atmos. Sci.*, *39*, 1026–1034.

Watanabe, S. (2008), Constraints on a non-orographic gravity wave drag parameterization using a gravity wave resolving general circulation model, *SOLA*, *4*, 61–64, doi:10.2151/sola.2008016.

Watanabe, S., K. Sato, and M. Takahashi (2006), A general circulation model study of orographic gravity waves over Antarctica excited by katabatic winds, *J. Geophys. Res.*, *111*, D18104, doi:10.1029/2005JD006851.

Watanabe, S., Y. Kawatani, Y. Tomikawa, K. Miyazaki, M. Takahashi, and K. Sato (2008), General aspects of a T213L256 middle atmosphere general circulation model, *J. Geophys. Res.*, *113*, D12110, doi:10.1029/2008JD010026.

————————————

Y. Kawatani, K. Miyazaki, and S. Watanabe, Frontier Research Center for Global Change, Japan Agency for Marine-Earth Science and Technology, 3173-25 Showa-machi, Kanazawa-ku, Yokohama city, Kanagawa 236-0001, Japan. (wnabe@jamstec.go.jp)

K. Sato, Department of Earth and Planetary Science, Graduate School of Science, University of Tokyo, Tokyo 113-0033, Japan.

M. Takahashi, Center for Climate System Research, University of Tokyo, Kashiwa 277-8568, Japan.

Y. Tomikawa, National Institute of Polar Research, Tokyo 190-8518, Japan.